2012

Three-dimensional transport imaging for the spatially resolved determination of carrier diffusion length in bulk materials

Blaine, K.E.

Three-dimensional transport imaging for the spatially resolved determination of carrier diffusion length in bulk materials

K. E. Blaine,[1] D. J. Phillips,[2] C. L. Frenzen,[3] C. Scandrett,[3] and N. M. Haegel[2]
[1]*Department of Mathematics, US Military Academy, West Point, New York 10996, USA*
[2]*Physics Department, Naval Postgraduate School, Monterey, California 93943, USA*
[3]*Applied Mathematics Department, Naval Postgraduate School, Monterey, California 93943, USA*

(Received 17 January 2012; accepted 11 March 2012; published online 6 April 2012)

A contact-free optical technique is developed to enable a spatially resolved measurement of minority carrier diffusion length and the associated mobility-lifetime ($\mu\tau$) product in bulk semiconductor materials. A scanning electron microscope is used in combination with an internal optical microscope and imaging charge-coupled device (CCD) to image the bulk luminescence from minority carrier recombination associated with one-dimensional excess carrier generation. Using a Green's function to model steady-state minority carrier diffusion in a three-dimensional half space, non-linear least squares analysis is then applied to extract values of carrier diffusion length and surface recombination velocity. The approach enables measurement of spatial variations in the $\mu\tau$ product with a high degree of spatial resolution. [http://dx.doi.org/10.1063/1.3698090]

I. INTRODUCTION

Minority carrier transport properties are generally strong indicators of semiconductor material quality and play a direct role in the performance of a wide range of devices, including solar cells, optical emitters such as light emitting diodes and lasers, photon sensors, nuclear radiation detectors, and some forms of transistors. Excess carriers, whether injected optically or via electrical contacts, must drift and/or diffuse to produce a signal. Since minority carrier transport depends on both carrier mobility and carrier lifetime, it is a sensitive and complex measure of material quality, depending on doping, point defect as well as dislocation density and surface recombination parameters.

Conventional approaches to measure minority carrier diffusion length include electron beam induced current (EBIC) (Ref. 1), its analog—optical-beam-induced current (OBIC) (Ref. 2), high-resolution scanning photocurrent,[3] interpretation of light-induced transient gratings,[4] or extraction from device performance models. These approaches have various strengths and limitations, but they generally require contacts or full device fabrication and are often limited in application to thin films and/or one-dimensional structures. Minority carrier diffusion lengths are also important, however, in devices, such as nuclear radiation detectors and some solar cells, where bulk material properties play a role. This may mean that the materials of interest are truly bulk in nature, such as nuclear radiation detectors that are generally millimeters if not centimeters in thickness, or that thin films are used where the diffusion lengths are comparable to or less than the film thickness.

We present here an instrument and the development of a modeling approach to allow minority carrier diffusion lengths to be determined for bulk materials from optical imaging of spatially resolved recombination luminescence. By combining a scanning electron microscope (SEM) for highly localized carrier generation, an optical microscope (OM), and a sensitive CCD array, this approach, known as transport imaging, can be applied with relatively high spatial resolution for materials characterization. Most importantly, the approach is contact-free and applicable to a wide range of luminescent materials.

II. TRANSPORT IMAGING FOR THE DETERMINATION OF THE $\mu\tau$ PRODUCT

Although transport imaging is related to cathodoluminescence (CL), there are fundamental differences between this approach and a range of scanning luminescence techniques. In both CL and transport imaging, the incident electron beam is used to create electron-hole pairs. In CL, however, the incident beam is commonly rastered over an area and all light created due to generation at a given point is mapped back to and assumed to be associated with that point. In that way, spatial imaging is tied to the motion of the generation source. While a large fraction of the luminescence from recombination does, in fact, occur at or very near the point of charge generation, the actual spatial variation in luminescence emission, whether from diffusion or drift of charge in a local field, is lost in conventional CL.

Transport imaging maintains the spatial variation of the recombination behavior by recording an image of the luminescence as the excitation source is either held fixed at a point or scanned repeatedly along a line. The approach is, to some extent, a highly spatially resolved version of the Haynes-Shockley experiment.[5] Transport imaging in the SEM allows for a direct two-dimensional steady-state visualization of diffusion behavior in a contact-free manor, applied here for the first time to bulk materials. For work in doped semiconductor samples, one can extract a minority carrier diffusion length L, which is then related to the mobility-lifetime ($\mu\tau$) product via

$$L = \sqrt{\frac{kT}{e}\mu\tau}. \quad (1)$$

The $\mu\tau$ product is an effective indicator of material quality, a critical device parameter for minority carrier devices such as lasers and certain transistors and a key parameter for assessing the uniformity of bulk materials for applications such as nuclear radiation detectors.

Previous transport imaging work in the SEM has been focused on diffusion in thin films and nanowires.[6–8] Application to bulk materials requires the development of a three-dimensional model for diffusion in a half space and multi-parameter fitting techniques to extract the relevant materials parameters. It is also more experimentally challenging because the spatial extent of the diffusion behavior for a given minority carrier diffusion length will be reduced due to the geometry. We describe the experimental approach and then develop the model for interpretation of the images from bulk materials.

III. EXPERIMENTAL APPROACH

The charge transport instrument combines two microscopes— a JEOL SEM for generating the non-equilibrium carrier population and an optical microscope for collecting and imaging the luminescence. The OM is on a retractable arm and can be positioned directly under the pole piece, with the electron beam passing through a small hole in the center of the first optical collecting surface. For transport imaging, the OM is used in a passive detection mode with a high sensitivity Apogee CCD camera. The CCD array size is 2184 × 1472 with pixels of 6.8 μm × 6.8 μm. The optical magnification is 20×, resulting in a effective scale in the optical image of 400 nm/pixel. Figure 1 shows a schematic of the system.

The SEM can be operated in any of three modes: spot, line, or picture. In work on the bulk materials, we utilize the line scan mode for generation. Picture mode is used to view the material for topographical uniformity and initial focusing of the optical image. Focusing is achieved by controlling the sample height with internal stage height adjustment. For this work, the energy of the electron beam was 20 keV, with probe currents from 3×10^{-10} to 6×10^{-12} A.

Variable temperature capability is achieved with a continuous flow of liquid helium through a cold stage. The sample is in vacuum and heat-sunk to a metal sample holder on the cold stage. Conductive silver paste is used for sample mounting. Temperatures from 300 to 5 K can be achieved.

Prior to transport imaging, standard CL spectroscopy is performed to identify the relevant luminescent signature. In this case, the CL shows the luminescence from bulk GaAs, with a room temperature peak emission at ≈870 nm. Because the materials are bulk, with no heterostructure barrier layers or added substrate material, the transport images can be collected broadband, with no requirement for filtering.

Figure 2 illustrates the progression of data acquisition for a sample case of room temperature bulk GaAs. Figure 2(a) shows the initial two-dimensional linescan (intensity as a function of position) captured by the CCD for a 15 s exposure, during which time the electron beam is rapidly scanned over the linear region as shown. The brighter luminescence at the bottom of the scan is due to the synchronization behavior of the SEM, which causes the beam to spend a slightly longer period of time at that position. This region of the data will not be used in the analysis. The spatial variation is shown in three dimensions in Figure 2(b). Finally, Figure 2(c) shows the intensity distribution perpendicular to the excitation line. In order to improve the signal-to-noise ratio, 100 individual distributions (individual pixel rows from the CCD) have been averaged. The small bump is an artifact due to reflection in the optical system. Since the result is symmetric, the analysis of the data for least squares fitting and extraction of the diffusion length will be done from the right-hand distribution to avoid this complication.

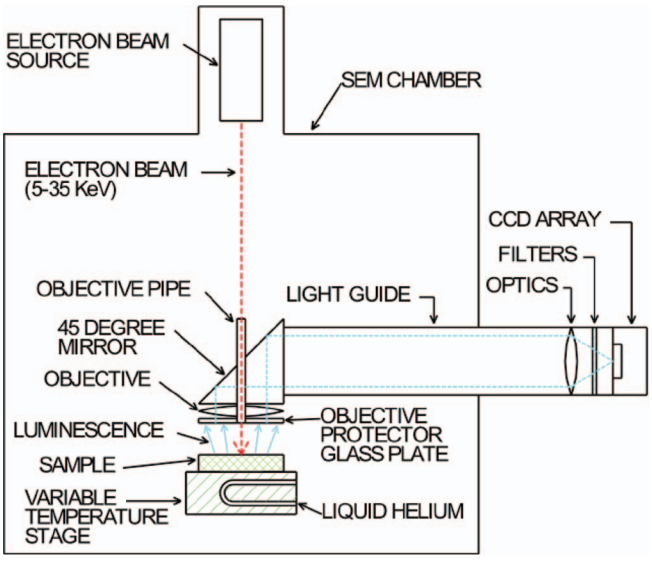

FIG. 1. Schematic of transport imaging system showing internal optical microscope and CCD imaging camera integrated with scanning electron microscope.

IV. DEVELOPMENT OF THE THREE-DIMENSIONAL DIFFUSION/RECOMBINATION MODEL

We now develop the governing equations for three-dimensional diffusion from a near-surface line source into an infinite half-space. We model the source as a delta function and use a Green's function to solve a diffusion equation with boundary conditions imposed by the free surface of the half space. To begin, consider an infinite half-space of semiconductor material with the following constant parameters:

D – diffusivity of the minority carriers in the bulk material (cm^2/s),
S – surface recombination velocity (cm/s),
τ – minority carrier recombination time (s),

and define $u(x, y, z)$ to be the concentration of excess carriers at any point (x, y, z) in the material and g to be the constant generation rate.

In steady state, we assume that the electron beam produces an infinite line source of excess carriers with generation rate g per unit distance along the line source (coinciding with the y-axis), as shown in Figure 3. We assume that the

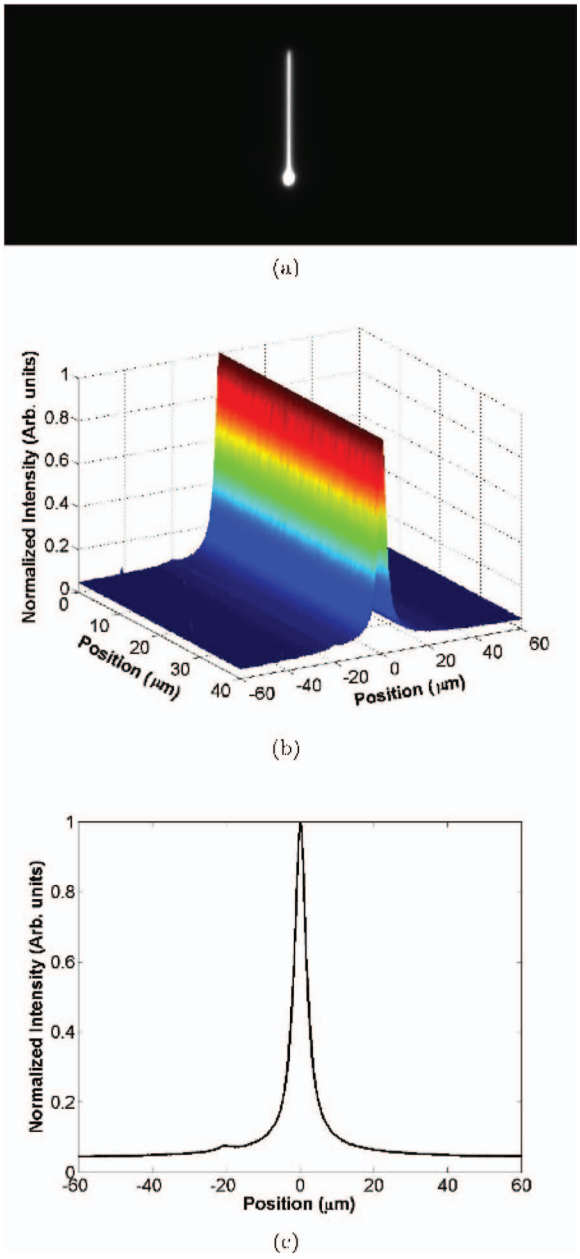

FIG. 2. Example of data acquisition and extraction. (a) 2D luminescence image created by line scan excitation on GaAs, (b) 3D presentation of the data illustrating spatial distribution of the luminescence perpendicular to the excitation, and (c) plot of average spatial distribution.

line source is uniform along the y direction so that the variations in carrier concentration due to diffusion will only be in the x and z directions. This means that u is a function of x, z only, $u = u(x, z)$. The problem then reduces to diffusion from a point source in the x-z plane. The source can now be modeled as a point at a depth z_o below the material surface, where z_o is determined primarily by the incident energy of the electron beam for a given target material. It is well known from Monte Carlo simulations and related experimental work that the incident electron beam produces a generation volume whose dimensions depend on the density and atomic number of the target material.[9] To account for this finite generation volume, we will fit the luminescence data beginning at some distance from the generation region. This is a reasonable

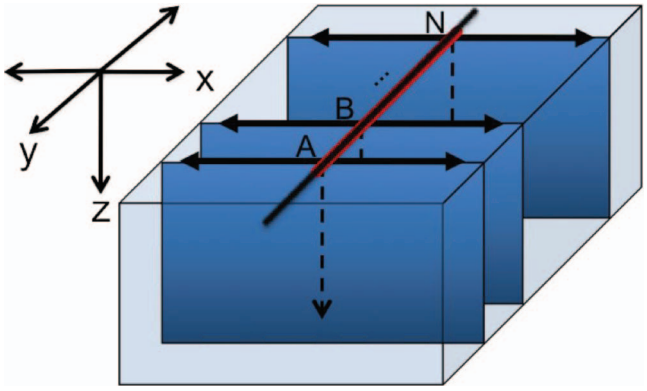

FIG. 3. Schematic of the three-dimensional excitation/diffusion model in the half space.

approximation, particularly for cases where L is significantly greater than the linear extent of the generation region.

Under the assumptions above, we can describe the source with strength g as a delta function

$$g \cdot \delta(x)\delta(z - z_0). \tag{2}$$

The carrier concentration $u(x, z)$ must satisfy the diffusion equation

$$\nabla^2 u(x, z) - \frac{1}{L^2} u(x, z) + \frac{g}{D}\delta(x)\delta(z - z_0) = 0 \text{ for } z > 0, \tag{3}$$

with boundary conditions given by

$$D \frac{\partial}{\partial z} u(x, z) = S u(x, z) \text{ at } z = 0 \tag{4}$$

and

$$u(x, z) \to 0 \quad \text{as} \quad \sqrt{x^2 + z^2} \to \infty. \tag{5}$$

Because the surface of the half-space is an unpassivated semiconductor surface, the boundary condition in Eq. (4) is used to relate the flux of minority carriers to the concentration present at the surface. The proportionality constant S in Eq. (4) has the dimensions of a velocity (the surface recombination velocity) and accounts for surface recombination effects. Finally, Eq. (5) models the extinction of the excess carrier population at increasing distances from the source in a bulk sample.

We rewrite the boundary condition in Eq. (4) as

$$\frac{\partial}{\partial z} u(x, z) = V\, u(x, z), \tag{6}$$

where

$$V = \frac{S}{D} \tag{7}$$

is a material parameter V with dimension 1/distance.

The solution of Eq. (3) alone, in the absence of the half-space boundary, is the free-space Green's function $u(r)$ and can be found using cylindrical symmetry and standard Green's function methods to be

$$u(r) = \frac{g}{2\pi D}\, K_0\left(\frac{r}{L}\right), \tag{8}$$

where K_0 is the zeroth-order modified Bessel function of the second kind and

$$r = \sqrt{x^2 + (z - z_0)^2}. \tag{9}$$

To solve the half-space problem including the boundary conditions, we Fourier transform equation (3) in x to obtain

$$\tilde{u}_{zz} - \left(\xi^2 + \frac{1}{L^2}\right)\tilde{u} = \frac{-g}{D}\delta(z - z_0), \tag{10}$$

where ξ is the Fourier transform variable. If we solve this and take the inverse Fourier transform, we obtain an integral representation of the free space Green's function as

$$u = \frac{g}{2\pi D}\int_{-\infty}^{\infty} \tfrac{1}{2\alpha} e^{-\alpha|z-z_0|} e^{-i\xi x}\, d\xi. \tag{11}$$

Equations (8) and (11) together give

$$K_0\left(\frac{r}{L}\right) = \int_{-\infty}^{\infty} \tfrac{1}{2\alpha} e^{-\alpha|z-z_0| - i\xi x}\, d\xi, \tag{12}$$

with

$$\alpha = \sqrt{\xi^2 + \frac{1}{L^2}}. \tag{13}$$

The general solution to Eq. (10) is

$$\tilde{u} = \begin{cases} Ae^{\alpha z} + Be^{-\alpha z_0}, & 0 \le z \le z_0, \\ Ce^{-\alpha z}, & z \ge z_0, \end{cases} \tag{14}$$

and the Fourier-transformed surface boundary condition is

$$\tilde{u}_z = V\tilde{u} \qquad \text{for} \quad z = 0, \tag{15}$$

while the jump condition across z_0 requires

$$-\alpha C e^{-\alpha z_0} - \{\alpha A e^{\alpha z_0} - \alpha B e^{-\alpha z_0}\} = \frac{-g}{D}. \tag{16}$$

The application of the boundary condition Eq. (15) to the general solution of Eq. (14) together with the jump condition at z_0 in Eq. (16) determines the values of A, B, and C as

$$A = \frac{g}{2\alpha D} e^{-\alpha z_0},$$

$$B = \frac{g}{2\alpha D}\left(\frac{\alpha - V}{\alpha + V}\right) e^{-\alpha z_0},$$

$$C = \frac{g}{2\alpha D}\left[e^{\alpha z_0} + \left(\frac{\alpha - V}{\alpha + V}\right) e^{-\alpha z_0}\right]. \tag{17}$$

We put the values for A, B, and C above into the general solution (Eq. (14)) and take an inverse Fourier transform to obtain the solution in the form

$$u(x,z) = \frac{g}{2\pi D}\int_{-\infty}^{\infty} \frac{1}{2\alpha} e^{\alpha|z-z_0| - i\xi x}\, d\xi + \frac{g}{2\pi D}\int_{-\infty}^{\infty} \frac{1}{2\alpha} e^{-\alpha(z+z_0) - i\xi x}\, d\xi - \frac{g}{\pi D}\int_{z_0}^{\infty} V e^{V(z_0-\zeta)} \int_{-\infty}^{\infty} \frac{1}{2\alpha} e^{-\alpha(z+\zeta) - i\xi x} d\xi\, d\zeta. \tag{18}$$

The free space Green's function relationship in Eq. (12) now allows us to rewrite Eq. (18) in the final form as

$$u(x,z) = \frac{g}{2\pi D}\left\{K_0\left(\frac{\sqrt{x^2 + (z - z_0)^2}}{L}\right) + K_0\left(\frac{\sqrt{x^2 + (z + z_0)^2}}{L}\right) - \int_{z_0}^{\infty} 2V e^{V(z_0-\zeta)} K_0\left(\frac{\sqrt{x^2 + (z+\zeta)^2}}{L}\right) d\zeta\right\}. \tag{19}$$

With the solution for the excess carrier distribution (Eq. (19)) as a function of x and z, we can relate this distribution to the resulting luminescence associated with carrier recombination. Some constant fraction of these carriers will recombine with majority carriers (electrons, in the case of n-type material), resulting in a luminescence distribution that reflects the minority carrier distribution. Because the peak luminescence in GaAs and other direct bandgap semiconductors occurs at a wavelength slightly below the wavelength associated with the direct bandgap, we expect photon emission from recombination events to occur at various depths z since the absorption edge drops off sharply for direct bandgap semiconductors. We integrate $u(x, z)$ with respect to z through the sample to account for the bulk nature of the recombination.

The integration in z of Eq. (19) gives $u(x)$, the integrated excess carrier distribution in the bulk material (carrier density per unit area) as a function of the distance x from the carrier generation source. This function $u(x)$ is

$$u(x) = A\left\{\int_{\frac{x}{L}}^{\infty} K_1(t)\sqrt{t^2 - \left(\frac{x}{L}\right)^2}\, dt + \int_{z_0}^{\infty} K_0\left(\frac{\sqrt{t^2 + x^2}}{L}\right)\frac{e^{V(z_0-t)} - 1}{L}\, dt\right\}, \tag{20}$$

where K_1 is the first-order modified Bessel function of the second kind and

$$A = \frac{gL}{\pi D}. \tag{21}$$

V. LEAST SQUARES ANALYSIS TO EXTRACT L

The least squares curve fitting is done using the Levenberg-Marquadt algorithm. L, V, and A are iteratively adjusted to minimize the residual sum of squares in the vector $\vec{p}$ using

$$\vec{p}_{i+1} = \vec{p}_i - (J^T J + \lambda\, \mathrm{diag}(J^T J))^{-1} J^T (u - \hat{u}(\vec{p})), \tag{22}$$

where u is the measured data from transport imaging, $\hat{u}(\vec{p})$ is the model curve fit, J is the Jacobian matrix $[\partial\hat{u}/\partial\vec{p}]$, and λ is the damping parameter in the Levenberg-Marquadt algorithm.

u has its first data point 10 μm from the source, as explained in Sec. IV. The cutoff for the data range is done just above the noise level. λ is adjusted up or down before each step to find the optimum direction for the step.

The size of each step is determined by evaluating $\vec{p}_{i+1}$ with different possible step sizes and fitting an interpolated polynomial to the residual error for each step size. Finding the minimum of this polynomial provides the next step size. This method allows for an increase or decrease in step size for subsequent iterations. Convergence to an optimal fit is considered complete once the step size has decreased so as to limit the changes in each of the parameters of $\vec{p}$ to less than 0.01% over nine iterative steps.

VI. EXPERIMENTAL RESULTS

Transport imaging was performed on two samples of high purity, metalorganic chemical vapor deposition (MOCVD)-grown GaAs. Sample 1 (S1) is a 50-μm thick epilayer that was grown on a semi-insulating GaAs substrate. At room temperature, Hall effect measurements indicated n-type material with a net doping of 1×10^{14} cm^{-3}. Sample 4 (S4) is also an n-type nominally 50 μm thick epilayer (also 1×10^{14} cm^{-3}) but grown on an n+ GaAs substrate. Independent time-resolved photoluminescence (TRPL) measurements gave a minority carrier lifetime of ~60 ns for S1, with the results for S4 beyond the maximum time constant limit for the system (>200 ns). The TRPL results are at best an estimate given system limitations, but they do indicate a minority carrier lifetime difference between the two samples. We attribute this to different defect densities based on the quality of material grown on different substrates, since the net doping levels, measured by the Hall effect, are not significantly different. This makes these samples a good choice for measuring minority carrier diffusion length and demonstrating bulk transport imaging.

Figure 4 presents the luminescence intensity profiles (logarithmic scale) as a function of position, perpendicular to the line source excitation, for a select number of temperatures for S1 (Figure 4(a)) and S4 (Figure 4(b)). Optical images were taken over a temperature range from 300 to 5 K for each sample. One hundred individual distributions (individual pixel rows from the CCD) have been averaged to obtain an average diffusion behavior over a distance of 40 μm on the material. The variation in the luminescence distribution with temperature indicates the effect of changes in diffusion length. One should note the variation in the x-axis scale for the two samples, indicating a significantly longer diffusion length for minority carriers in sample 4.

Figure 5 shows an example of three of the distributions, where the dots are the experimental data points and the lines indicate the modeling result obtained from the least squares fitting of data to Eq. (20) as described in Sec. V. In order to test the convergence behavior, multiple least squares analyses were performed, with variations in the starting values for the parameters L, V, and A. As one representative example, 20 different simulations were performed, with variations in initial parameters, for the 300 K measurement on sample 4. The results give a mean L of 14.07 μm, with a standard deviation based on the 20 different starting points, of 3.1×10^{-2} μm.

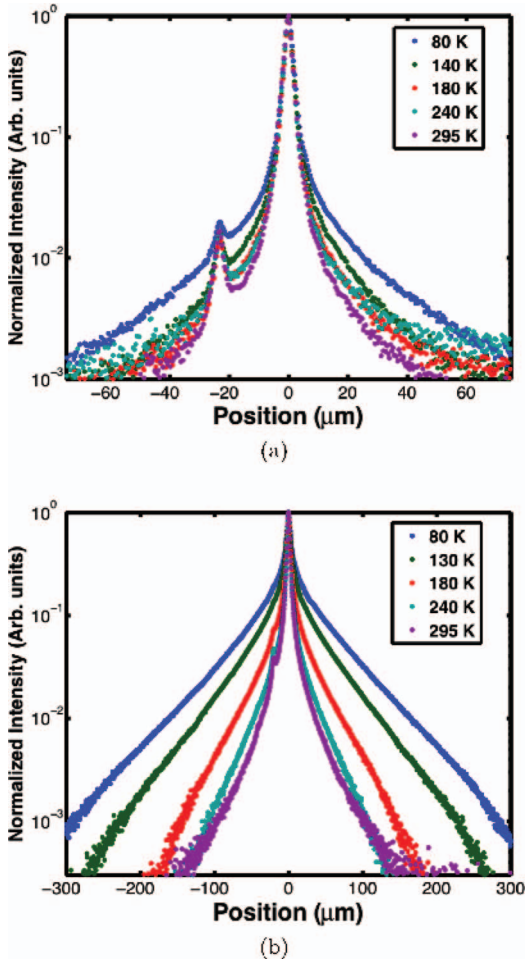

FIG. 4. Luminescence intensity as a function of position, perpendicular to the excitation region for (a) sample 1 and (b) sample 4. A select number of temperatures are presented from a much larger variable temperature study.

Figure 6 shows the best fit values for L as a function of temperature for S1 and S4. We observe an increase with decreasing temperature at higher temperatures and then a much weaker temperature dependence below about 80 K. Since the

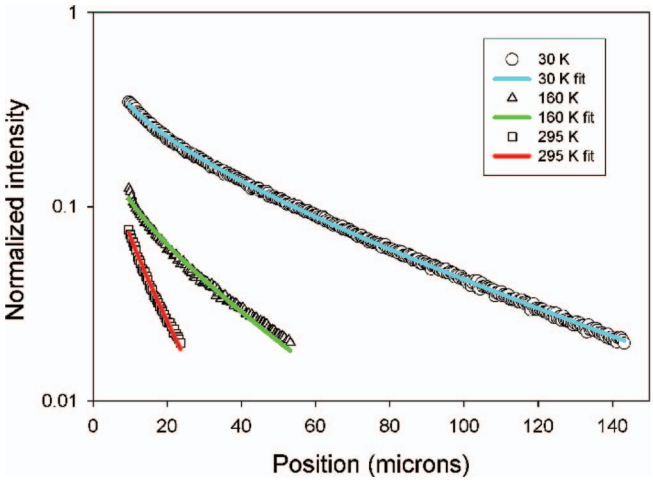

FIG. 5. Examples of comparison of the optimum model distribution (lines), based on least squares fitting of the data, to the experimental results for sample S4 (points). The fitting is started 10 μm from the peak intensity, to avoid interference from generation volume effects.

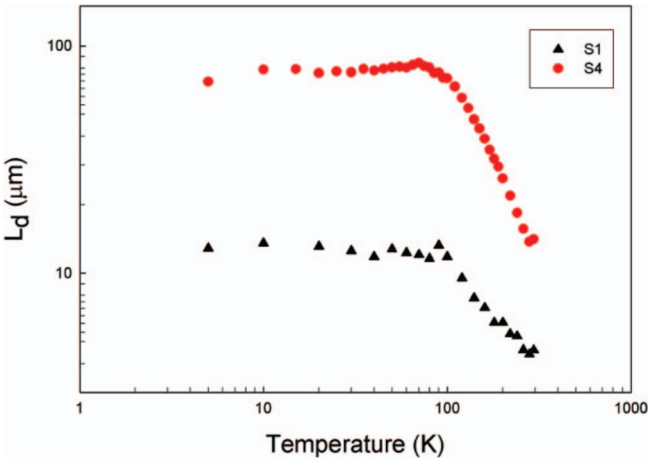

FIG. 6. Minority carrier diffusion length L_d as a function of temperature for S1 and S4.

diffusion length includes the $\sqrt{T}$ dependence associated with the diffusivity, we account for that and replot the data in Figure 7 as the more direct material parameter $\mu\tau$ as a function of temperature.

In order to further investigate the temperature-dependent behavior, the measurements were repeated, with varying probe current and heat sinking strategies to reduce any potential effects of local sample heating. No significant variations were found. It is also important to note that the diffusion length in S4 at lower temperatures does approach the actual thickness of the sample, which would be a limitation of the model for these particular epitaxial layers. We see, however, that S1 also displays a similar temperature-dependent behavior, indicating that epilayer thickness is not the cause for the insensitivity of L to temperature at lower temperatures. Instead, it results from the balance of the weaker $\mu\tau$ dependence at lower temperatures with the $\sqrt{T}$ factor. Limited data exist for the temperature dependence of minority carrier lifetime, but early work on single-crystal GaAs, based on photoconductivity and the photomagnetic effect, found minority hole lifetime to be basically temperature independent over the range from 300 to 80 K in more heavily doped material.[10] At the low dopant concentrations here, however, there is little knowledge of the behavior of bulk samples or thick films, because such high purity samples have not been easily available in these forms.

Although the results presented in Figures 6 and 7 were averaged over a ~40 μm region to provide an average material parameter, the transport imaging technique has the potential to provide high-resolution mapping of L and the $\mu\tau$ product. Since each pixel corresponds to a distance of 400 nm on the sample, mapping of the $\mu\tau$ product can, in principle, be done at that scale if the signal to noise for a single luminescence distribution is sufficient. This approach has been demonstrated in a thin film to measure the variations in transport properties associated with dislocation networks in lattice mismatched structures.[11]

Figure 8 shows the spatial variation determined for S1 and S4 as a function of position at 300 K, using a running average approach in which an average of 40 pixels has been used for the least squares analysis. We plot the minority carrier diffusion length as a function of position over a distance of 40 μm. The materials show variations in L that could be associated with either growth fluctuations in the epitaxial layer or variations in the substrate material that propagate into the epitaxial layer. Since the materials are grown by MOCVD, some degree of spatial variation can be expected due to the the growth process. In sample S1, it is more likely that the variations reflect variations in the semi-insulating substrate.

For bulk materials, no other technique can provide this level of spatial resolution for local transport properties. Standard analysis of EBIC profiles, which is the traditional way to obtain minority carrier diffusion lengths, is limited to the near-contact region and requires the assumption that L remains constant over the range of interest. In materials designed for use in nuclear radiation detectors, spatially resolved information on the $\mu\tau$ product has been obtained via mapping of detector responses with high energy excitation.[12,13] These approaches, however, do not yet provide the spatial resolution that can be obtained with transport

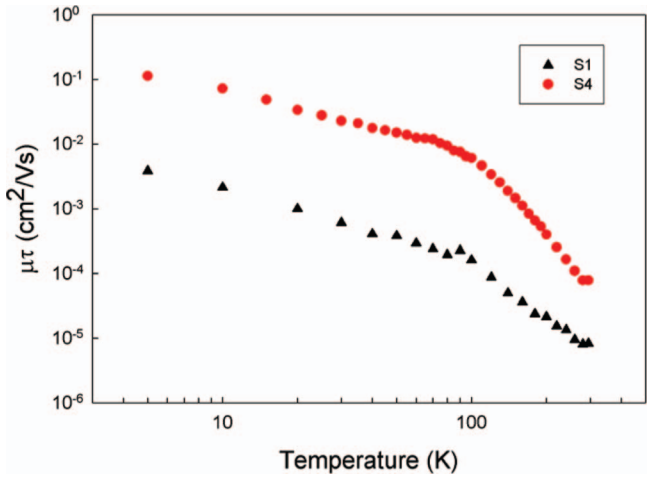

FIG. 7. Mobility-lifetime ($\mu\tau$) product as a function of temperature for S1 and S4.

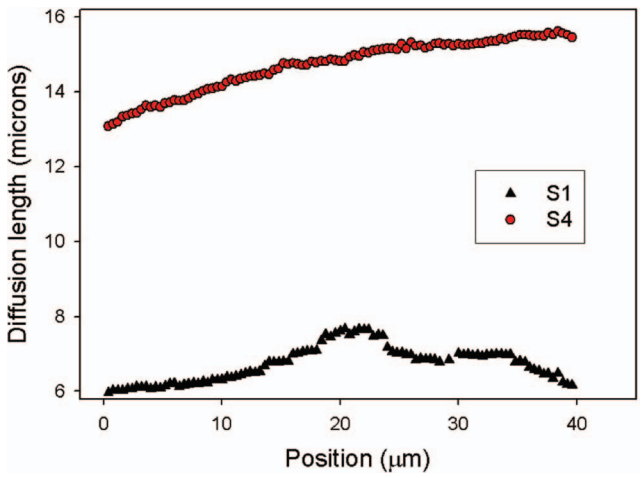

FIG. 8. Spatial variation of L_d (300 K) as a function of position.

imaging and both require device fabrication and testing to correlate to transport properties. This optical technique therefore has the potential for impact on the characterization of materials for nuclear radiation detectors to simultaneously measure the $\mu\tau$ product and its spatial variation, both of which are critical to device performance.

VII. CONCLUSION

In summary, we have demonstrated the application of a measurement technique to determine electronic transport parameters (minority carrier diffusion length and the associated $\mu\tau$ product) by imaging the luminescence distribution created by a line source excitation on the surface of a bulk material. This approach allows for a contact-free method to extract the local diffusion length from a single optical image. A three-dimensional transport model has been presented for the diffusion behavior and applied, using a least squares fitting analysis, to extract spatially resolved transport parameters. The technique has been applied to thick films of high purity GaAs to demonstrate the effect of the growth substrate on carrier lifetime and diffusion length. Future work will focus on extraction of the surface recombination velocity, both spatially and as a function of temperature.

ACKNOWLEDGMENTS

This work was supported by the Academic Research Initiative (ARI) of DHS through Interagency Agreement HSHQDC-11-X-0015. The graphic in Figure 2 was created by J. Adeff.

[1]H. J. Leamy, J. Appl. Phys. **53**, R51 (1982).
[2]T. Wilson and C. Sheppard, *Scanning Optical Microscopy* (Academic, London, 1984).
[3]J. W. P. Hsu, Mate. Sci. Eng. **33**, 1 (2000).
[4]H. J. Eichler, P. Gunter, and D. W. Pohl, *Laser-Induced Dynamic Gratings* (Springer, Berlin, 1986).
[5]J. R. Haynes and W. Shockley, Phys. Rev. **81**, 835 (1951).
[6]D. R. Luber, F. M. Bradley, N. M. Haegel, M. C. Talmadge, M. P. Coleman, and T. D. Boone, Appl. Phys. Lett. **88**, 163509 (2006).
[7]N. M. Haegel, T. J. Mills, M. Talmadge, C. Scandrett, C. L. Frenzen, H. Yoon, C. M. Fetzer, and R. R. King, J. Appl. Phys. **105**, 023711 (2009).
[8]L. Baird, C. P. Ong, R. A. Cole, N. M. Haegel, A. A. Talin, Q. Li, and G. T. Wang, Appl. Phys. Lett. **98**, 132104 (2011).
[9]J. Goldstein, D. Newbury, D. Joy, C. Lyman, P. Echlin, E. Lifshin, L. Sawyer, and J. Michael, *Scanning Electron Microscopy and X-Ray Microanalysis* (New York, Kluwer, 2000); also see the discussion in Ref. 1.
[10]A. V. Dudenkov and V. V. Nikitin, Sov. Phys. Solid State **8**, 2432 (1967).
[11]N. M. Haegel, S. E. Williams, C. L. Frenzen, and C. Scandrett, Semicond. Sci. Technol. **25**, 055017 (2010).
[12]A. Lohstroh, P. J. Sellin, and A. Simon, "High-resolution mapping of the mobility-lifetime product in CdZnTe using a nuclear microprobe," J. Phys. Condens. Matter **16**, S67–S73 (2004).
[13]M. Amman, J. S. Lee, P. N. Luke, H. Chen, S. A. Awadalla, R. Redden, and G. Bindley, IEEE Trans. Nucl. Sci. **56**, 795–799 (2009).